Arredondo, F., et al. Stability improvement of a transmission grid with high share of renewable energy using TSCOPF and inertia emulation. In: *IEEE Transactions on Power Systems 37(4), July 2022, Pp. 3230-3237*

DOI: https://doi.org/10.1109/TPWRS.2020.3022082

Stability Improvement of a Transmission Grid with High Share of Renewable Energy using TSCOPF and Inertia Emulation

Francisco Arredondo, Pablo Ledesma, Edgardo D. Castronuovo, *Senior Member, IEEE,* and Mohammad Amin Aghahassani

***Abstract*-- This paper proposes a Transient Stability Constrained Optimal Power Flow (TSCOPF) formulation that models non-synchronous renewable generation equipped with synthetic inertia. The proposed optimization problem calculates the optimal operating point of the system, accommodating high shares of non-synchronous renewable generation while ensuring transient stability in the event of critical incidents. Synthetic inertia controllers are used to improve the dynamic stability of the system in cases of very high share of renewable generation. The proposed tool is tested in the North-West Spanish system, a network with a high penetration of wind energy that causes a reduction in the total system inertia. The results of the study show that 1) synthetic inertia in renewable power plants can diminish electromechanical oscillations after a severe contingency, reducing the cost of ensuring transient stability; 2) using synthetic inertia the system becomes more stable when conventional generation is decommissioned following de-carbonization and renewable promotion policies; and 3) the proposed model can be used to calculate the parameters of the synthetic inertia control.**

***Index Terms*-- nonlinear programming, optimal power flow, power system transient stability, renewable generation, inertia emulation.**

NOMENCLATURE

A. Abbreviations

COI	Center of Inertia
GAMS	General Algebraic Modeling System
IPOPT	Interior Point Optimizer
MU	Monetary Units
OPF	Optimal Power Flow
PCC	Point of Common Coupling
PF	Pre-Fault
PLL	Phase-Locked Loop
PSSE	Power System Simulator for Engineering
PV	Solar Photovoltaic
ROCOF	Rate of Change of Frequency
TD	Time Domain.
TSCOPF	Transient Stability Constrained Optimal Power Flow.
TSO	Transmission System Operator

B. Indices and sets

i,j	Index for nodes
t	Index for time periods
Ω^{B}	Set of buses of the power system
Ω^{G}	Set of the synchronous generation units
Ω^{NSG}	Set of the renewable non-synchronous generation units
Ω^{L}	Set of loads
Ω^{T}	Set of the time periods corresponding to the pre-fault, fault and post fault stages
Ω^{TD}	Set of the time periods corresponding to the fault and post fault stages
Ω^{TDELAY}	Set of the time periods corresponding to the delay of the frequency measurement

C. Parameters

A^{G}, B^{G}, C^{G}	Fuel cost coefficients of the power plants [MU/MWh]
A^{P}, B^{P}, C^{P}	Active power coefficients of the ZIP load model
A^{Q}, B^{Q}, C^{Q}	Reactive power coefficients of the ZIP load model
D^{BUS}	Value of the of element (i,j) of the frequency divider formula matrix [p.u.]
H^{EMU}	Synthetic inertia constant of a non-synchronous renewable power plant [s]
$I^{L,MAX}$	Upper limit of the current in lines and transformers. [p.u.]
P^{L}, Q^{L}	Active and reactive nominal load [p.u.]
P^{REF}	Available non-synchronous generation power [p.u.]
Q^{REF}	Reactive power injected by a non-synchronous renewable power plant in the steady state operation [p.u.]
T^{IE}	Synthetic inertia time constant [s]
V^{CON}	Limit of under-voltage ride through [p.u.]
V^{MIN}, V^{MAX}	Limits of the bus voltage [p.u.]
$Y_{i,j}$	Absolut value of the element (i,j) of the bus admittance matrix [p.u.]
$\Delta p^{MIN,NSG}$	Lower limit of the active power variation of a non-synchronous renewable power plant [p.u.]
$\Delta p^{MAX,NSG}$	Upper limit of the active power variation of a non-synchronous renewable power plant [p.u.]
Δt	Integration time step [s]
$\Delta\omega^{MAX}$	Limit of the speed deviation of a synchronous power plant [p.u.]
$\theta_{i,j}$	Phase of the element (i,j) of the bus admittance matrix [p.u.]
δ^{MAX}	Limit of the rotor angle deviation of a synchronous power plant [rad]
ω^{REF}	Frequency reference of the grid [rad/s]

D. Variables

f^{CON}	Binary variable that is equal to 1 if renewable power plant remains connected, and 0 otherwise

f^{CURTAIL}	Non-synchronous renewable curtailment factor
f^{LV}	Low voltage correction factor
i^{L}	Current between nodes (i,j) [p.u.]
$p^{\mathrm{G}}, q^{\mathrm{G}}$	Active and reactive power output of a synchronous power plant [p.u.]
$p^{\mathrm{NSG}}, q^{\mathrm{NSG}}$	Active and reactive power output of a non-synchronous renewable power plant [p.u.]
$p^{\mathrm{L}}, q^{\mathrm{L}}$	Active and reactive load
q^{VS}	Reactive power variation during a voltage dip by a non-synchronous renewable power plant [p.u.]
$ROCOF$	Rate of Change of Frequency at bus [p.u.].
v	Bus voltage magnitude [p.u.]
α	Phase of the bus voltage [rad]
Δf	Frequency deviation at bus [p.u.]
Δf^{D}	Frequency deviation measurement at bus [p.u.]
Δp^{NSG}	Active power variation of a non-synchronous renewable power plant [p.u.]
$\Delta\omega^{\mathrm{COI}}$	Speed deviation of the center of inertia [p.u.]
δ	Rotor angle of a synchronous power plant [rad]
δ^{COI}	Rotor angle of the center of inertia [rad]

I. Introduction

The transition towards a 100% renewable electric power system involves the replacement of conventional synchronous power plants with non-synchronous renewable generation, reducing the inertia of the system and affecting transient stability [1]. In these new scenarios, additional control strategies for non-synchronous renewable generation must be evaluated and implemented to maintain adequate levels of security and reliability. In this context, TSCOPF emerges as an effective tool to calculate the optimal operation of a power system while ensuring its stability.

TSCOPF is a non-linear optimization problem that includes in the same structure the static representation of the system in normal operation and the dynamic simulation of the system during and after a contingency. The solution of a TSCOPF ensures 1) an economical and secure steady-state operation of the power system; and 2) that the system remains stable in the event of one or several critical contingencies. During the last decade various approaches have been proposed to address this problem. References [2]–[5] review the different methods and their contributions in detail.

Previous TSCOPF studies consider the dynamic representation of conventional synchronous generation, but often neglect non-synchronous renewable energy sources. Traditionally, the inertial response of energy systems has been given by large synchronous power plants, as they contain a large rotating mass directly connected to the system. Non-synchronous renewable sources do not provide inertia since they decouple the grid from the electrical generator via electronic interfaces [6]. Consequently, scenarios with high shares of non-synchronous renewable sources reduce the total inertia, which can make the system more unstable under critical contingencies.

Recently, a growing number of studies propose that non-synchronous renewable power plants should emulate inertia to improve the dynamic stability [7]–[9]. Virtual inertia controllers can provide inertia to the system by modifying the active power output proportionally to the derivative of the network frequency or Rate of Change of Frequency (ROCOF) at the connection point [10]–[12]. Previous studies have proposed the use of synthetic inertia mainly to solve frequency stability problems, but rarely in transient stability studies.

This work expands TSCOPF formulations to represent non-synchronous renewable generation and storage systems with controls that depend on the frequency and the voltage at their Point of Common Coupling (PCC). The proposed algorithm calculates the voltages, and using the frequency divider formula proposed in [13], the frequency in each bus of the system and at each sample time. Using this new feature, the proposed tool represents the control of inverters of non-synchronous power parks that provide synthetic inertia.

The main contributions of this paper are:

- A software tool is implemented and tested to optimize the operation of energy systems with very high share of non-synchronous renewable generation, that considers dynamic security constraints.
- An economic study of the cost of ensuring transient stability in 100% renewable scenarios with very high penetration of non-synchronous renewable generation.
- An evaluation of the effect of inertia emulation on transient stability, power dispatch and total generation cost.

The proposed algorithm is applied to the North West Spanish power network, around the region of Galicia. Due to its long coast and its mountainous geography, this system hosts a large number of wind and hydro power plants [14]. Currently its operation involves scenarios in which the production from renewable sources connected to the network through electronic converters exceeds the production from conventional power plants [15]. In the near future, non-synchronous generation will increase its share in the system due to de-carbonization and renewable promotion policies.

The rest of the paper is organized as follows: Section II describes the optimization model; Section III describes the case study; Section IV presents and discusses the results; and Section V concludes the paper.

II. Optimization model

The optimization model proposed here is composed of 1) the objective function (1) that minimizes the total generation cost of the system and 2) the set of equality and inequality constraints that is summarized in Table I and models both the steady state and the dynamic behavior of a system during the fault and post-fault stages. Equations in italics are presented in previous papers [16], [17], while non-italic equations are new and discussed in the following sections. The solution of this model provides the most economic operation point of a system maintaining, on the one hand, static constraints such as limits in power plant production, bus voltages limits and line currents and, on the other hand, ensuring transient stability in the event of a critical incident.

$$\min \quad \mathrm{f}(p^{\mathrm{G}}_{i,0}) = \sum_{\forall i \in \Omega^{\mathrm{G}}} (\mathrm{A}^{\mathrm{G}}_i (p^{\mathrm{G}}_{i,0})^2 + \mathrm{B}^{\mathrm{G}}_i p^{\mathrm{G}}_{i,0} + \mathrm{C}^{\mathrm{G}}_i) \tag{1}$$

This article has been accepted for publication in a future issue of this journal, but has not been fully edited. Content may change prior to final publication. Citation information: DOI 10.1109/TPWRS.2020.3022082, IEEE Transactions on Power Systems

TABLE I
SUMMARY OF CONSTRAINTS OF THE OPTIMIZATION PROBLEM

Component	Equality Constraints	Inequality Constraints
Network and loads	Power flow equations: Eqs. (2)-(3) *Load equations: Eqs. (6)-(7) in* [17]. *Currents in branches and transformers: Eqs.(4) in [16].*	*Voltage limits at buses, limits on power generation, and maximum currents throught branches and transformers: Eqs. (3) and (5) in [16].*
Conventional generation	*Discretized algebraic equations of power plants: Eqs. (6)-(13) in [16].* *Power plant static equations: Eqs.(15)-(19) in [16]*	*Field voltage limits: Eq. (14) in [16].*
Frequency calculation	Frequency divider: Eq. (4) Delay due to the frequency measurement: Eq.(16)-(17)	
Non-synchronous generation	Active/reactive power generation: Eqs. (5)-(6) Fault ride through capability: Eq. (7) Synthetic inertia control and calculation of ROCOF: Eq. (10)-(17)	
Stability limits	*Calculation of the COI angle: Eq. (18)*	*Maximum deviation of rotor angles with respect to the COI angle: Eq.(19)*

A. Network and load modeling

The power balance for each bus *i* and time sample *t* models the network using the following equations:

$$p_{i,t}^{\mathrm{G}} + f_{i,t}^{\mathrm{LV}} p_{i,t}^{\mathrm{NSG}} - f_{i,t}^{\mathrm{LV}} p_{i,t}^{\mathrm{L}} = v_{i,t} \sum_{j=1}^{j=\mathrm{N}} v_{j,t} \mathrm{Y}_{i,j} \cos(\alpha_{i,t} - \alpha_{j,t} - \theta_{i,j}), \forall i \in \Omega^{\mathrm{B}}, \forall t \in \Omega^{\mathrm{T}} \quad (2)$$

$$q_{i,t}^{\mathrm{G}} + f_{i,t}^{\mathrm{LV}} q_{i,t}^{\mathrm{NSG}} - f_{i,t}^{\mathrm{LV}} q_{i,t}^{\mathrm{L}} = v_{i,t} \sum_{j=1}^{j=\mathrm{N}} v_{j,t} \mathrm{Y}_{i,j} \sin(\alpha_{i,t} - \alpha_{j,t} - \theta_{i,j}), \forall i \in \Omega^{\mathrm{B}}, \forall t \in \Omega^{\mathrm{T}} \quad (3)$$

where terms $p_{i,t}^{G}$ and $q_{i,t}^{G}$ represent the active and reactive power injected by a synchronous power plant, and $p_{i,t}^{\mathrm{NSG}}$ and $q_{i,t}^{\mathrm{NSG}}$ the active and reactive power injected by a non-synchronous power park. Variables $v_{i,t}$ and $v_{j,t}$ are the absolute values of the voltage at bus *i* or *j*, while variables $\alpha_{i,t}$ and $\alpha_{j,t}$ represent the angle of the complex voltage at bus *i* or *j*. Parameters $Y_{i,j}$ and $\theta_{i,j}$ are magnitude and angle of the term of the bus admittance matrix in the *(i,j)* position, respectively. Correction factors $f_{i,t}^{LV}$ are included to achieve numerical convergence during severe faults that cause low voltages close to zero. Its use is a common practice in transient stability simulations[18]-[19], taking a value of 1 at normal voltages and decreasing quadratically towards zero when the magnitude of the voltage is very low. Terms $p_{i,t}^{L}$ and $q_{i,t}^{L}$are the system loads, represented by a ZIP load model composed of a constant power, a constant current, and a constant impedance.

B. Calculation of the frequency at the nodes of the system

The calculation of the frequency in all the buses of the system is required to model frequency controls in non-synchronous power parks and energy storage systems, as well as frequency-dependent loads. Traditionally, two approaches have been used. The first one is the calculation of the frequency of the Center of Inertia (COI) from the speed of the synchronous power plants. While the COI is easy to calculate in centralized approaches, it is no useful to represent local oscillations and consequently not adequate to define controls based on frequency measurements. The second approach is the use of a phase-locked loop (PLL) to measure the derivative of the bus voltage angle, which has been demonstrated as a valid technique to measure local oscillations. However, the complexity of its implementation in optimization problems and its well-known numerical issues make it unsuitable for simultaneous discretization TSCOPF models [20].

The frequency divider formula, firstly proposed in [13], has recently proved to be a simple and reliable approach to estimate the frequency in all the buses of the system. Reference [20] analyses different bus frequency estimators for transient stability studies and shows that the frequency divider formula is consistent and captures properly local oscillations. Furthermore, reference [21] validates the frequency divider formula using a real-time digital simulator with physical PMUs connected in the loop. Equation (4) implements the frequency divider formula in the proposed TSCOPF model by calculating the frequency deviation at each bus and each sample time as a function of the speed deviation of the synchronous generators and the matrix of parameters $\mathrm{D}_{i,j}^{\mathrm{BUS}}$. Matrix $\mathrm{D}^{\mathrm{BUS}}$ is calculated using the network admittances and the synchronous machine internal impedances, as explained in [13].

$$\Delta f_{i,t} = \sum_{\forall j \in \Omega^{G}} \mathrm{D}_{i,j}^{\mathrm{BUS}} \Delta \omega_{j,t}, \forall i \in \Omega^{B}, \forall t \in \Omega^{\mathrm{T}} \quad (4)$$

C. Modeling of non-synchronous power parks

Renewable sources connected to the grid through electronic converters are increasingly used in modern power systems and must therefore be properly accounted for in TSCOPF models. This section proposes a non-synchronous power park model (5)-(7), together with its controllers (10)-(17), that is adequate for the representation of this kind of sources in simultaneous discretization TSCOPF problems. The proposed model is suitable for both variable speed windmills and PV sources.

Equations (5) and (6) represent the active and reactive power injected to the grid by a non-synchronous renewable power plant at each sample time:

$$p_{i,t}^{\mathrm{NSG}} = f_i^{\mathrm{CON}} (\mathrm{P}_i^{\mathrm{REF}} + \Delta p_{i,t}^{\mathrm{NSG}}) \frac{v_{i,t}}{v_{i,0}}, \forall i \in \Omega^{\mathrm{NSG}} \forall t \in \Omega^{\mathrm{TD}} \quad (5)$$

$$q_{i,t}^{\mathrm{NSG}} = f_i^{\mathrm{CON}} \mathrm{Q}_i^{\mathrm{REF}} \frac{v_{i,t}}{v_{i,0}}, \forall i \in \Omega^{\mathrm{NSG}} \forall t \in \Omega^{\mathrm{TD}} \quad (6)$$

Non-synchronous power parks are represented as a controlled current source because the response time of the power electronics and their controllers is short compared to the time scale of the transient stability studies [22]. Parameters P_i^{REF} and Q_i^{REF} represent the scheduled active and reactive power injected by the renewable module during steady state operation. Variable $\Delta p_{i,t}^{NSG}$ represents the dynamic response of the active power given by a controller during the time domain. Finally, variable f_i^{CON} is calculated in (7) and models the fault ride through capability of renewable sources, which disconnects the power plant when the voltage dip at the point of common coupling exceeds the low voltage limits given by the corresponding grid code [23]. In the pre-fault stage, variable f_i^{CON} takes always the value 1.

$$f_i^{CON} = \begin{cases} 1 & if\ v_{i,t} \geq V^{CON}, \forall i \in \Omega^{NSG} \forall t \in \Omega^{TD} \\ 0 & if\ v_{i,t} \leq V^{CON}, \forall i \in \Omega^{NSG} \forall t \in \Omega^{TD} \end{cases} \quad (7)$$

This work evaluates the impact of a synthetic inertia control on transient stability. The modeled control follows the ROCOF at the point of common coupling and modifies the active power set point using (8). The controller is a control loop added to the power converter that creates an active power control signal following the approach in [10], [11]. The ROCOF is calculated by (9) at each bus and at each sample time by using the frequency deviation calculated in (4).

$$\frac{d\Delta p_i^{NSG}}{dt} = -\frac{1}{T_i^{IE}}(2\omega^{REF} H_i^{EMU} ROCOF_i + \Delta p_i^{NSG}) \quad (8)$$

$$\frac{d\Delta f_i}{dt} = ROCOF_i \quad (9)$$

To include differential equations (8) and (9) in the optimization problem they are discretized using the trapezoidal rule, which results in (10) and (13), respectively. Constraints (11) and (12) are the upper and lower limits of the active power variation. Finally, constraints (14) and (15) result from equaling to zero equations (8) and (9) to initialize variables Δp_i^{NSG} and $ROCOF_i$ in the pre-fault stage.

$$\begin{aligned} &\Delta p_{i,t}^{NSG}\left(1+\Delta t/2T_i^{IE}\right) - \Delta p_{i,t-1}^{NSG}\left(1-\Delta t/2T_i^{IE}\right) \\ &= -\left(2\omega^{REF} H_i^{EMU} ROCOF_{i,t} \Delta t/2T_i^{IE}\right) \\ &-\left(2\omega^{REF} H_i^{EMU} ROCOF_{i,t-1} \Delta t/2T_i^{IE}\right), \forall i \in \Omega^{NSG} \forall t \in \Omega^{TD} \end{aligned} \quad (10)$$

$$\Delta p_{i,t}^{NSG} = \min[\Delta p_{i,t}^{NSG}, \Delta P_i^{MAX,NSG}] \forall i \in \Omega^{NSG} \forall t \in \Omega^{TD} \quad (11)$$

$$\Delta p_{i,t}^{NSG} = \max[\Delta p_{i,t}^{NSG}, \Delta P_i^{MIN,NSG}] \forall i \in \Omega^{NSG} \forall t \in \Omega^{TD} \quad (12)$$

$$\begin{aligned} &\Delta f_{i,t}^{D} - \Delta f_{i,t-1}^{D} \\ &= 0.5\Delta t(ROCOF_{i,t} + ROCOF_{i,t-1}), \forall i \in \Omega^{NSG} \forall t \in \Omega^{TD} \end{aligned} \quad (13)$$

$$\Delta p_{i,0}^{NSG} = 0, \forall i \in \Omega^{NSG} \quad (14)$$

$$ROCOF_{i,0} = 0, \forall i \in \Omega^{NSG} \quad (15)$$

The delay due to the frequency measurement and the phase-locked loop can cause significant variations in the response of the inertia controller and must therefore be properly accounted for [10]. This study models this delay using constraints (16) and (17).

$$\Delta f_{i,t}^{D} = \Delta f_{i,t-DELAY} \forall i \in \Omega^{NSG} \forall t \notin \Omega^{TDELAY} \quad (16)$$

$$\Delta f_{i,t}^{D} = 0, \forall i \in \Omega^{NSG}, \forall t \in \Omega^{TDELAY} \quad (17)$$

D. Modeling of conventional power plants and neighboring power systems

Synchronous power plants are modeled using the well-known 4th order d-q synchronous generator model [24], [25].

Neighboring power systems are crucial to enhance inertia and stability in interconnected grids, and consequently, to increase the share of non-conventional renewable generation securely. In this study, the neighboring systems are reduced to an equivalent bus with a constant power load and a synchronous generator with an inertia equal to the aggregated inertia of the corresponding system. The load minus the generation in the equivalent bus is the power exported by the studied system, which can take a positive or negative value depending on the direction of the power flow.

E. Stability criterion

The transient stability criterion is defined as the deviation of the machine rotor angle from its center of inertia reference [2]. Constraints (18) limit the local rotor angle deviation of each generator with respect to the COI angle. This restriction prevents local deviations of synchronous generators from exceeding a certain limit, which could cause one or more power plants to lose synchronism. Constraint (19) calculates the COI angle to apply the stability criterion in (18).

$$-\delta^{MAX} \leq \delta_{i,t} - \delta_t^{COI} \leq \delta^{MAX}, \forall i \in \Omega^{G}, \forall t \in \Omega^{T} \quad (18)$$

$$\delta_t^{COI} = \left(\sum_{\forall i \in \Omega^{SG}} H_i \delta_{i,t}\right) / \left(\sum_{\forall i \in \Omega^{SG}} H_i\right), \forall t \in \Omega^{T} \quad (19)$$

III. Description of the Study Case and Implementation

This study is carried out in the North-West Spanish power system, a transmission grid that is interconnected to the Spanish system to the east and the Portuguese system to the south, and borders the Atlantic Ocean to the west and the Cantabrian Sea to the north along 1,500 km of coastline. Its geographical location puts it in direct contact with strong winds coming from the Atlantic Ocean. Due to its strategic location, the system has

This article has been accepted for publication in a future issue of this journal, but has not been fully edited. Content may change prior to final publication. Citation information: DOI 10.1109/TPWRS.2020.3022082, IEEE Transactions on Power Systems

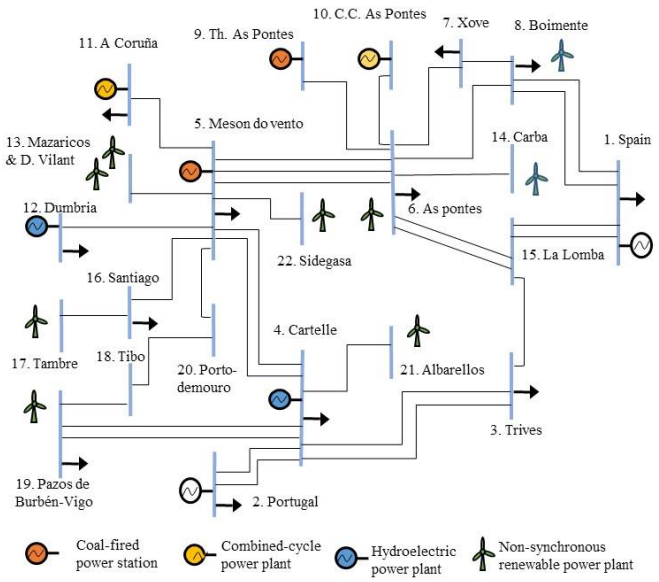

Fig. 1 North West Spanish power system.

become an optimal area for the installation of wind farms.

Fig. 1 shows the one-line diagram of the transmission system with the main power plants and loads. Generation is mainly provided by six conventional power plants and eight non-conventional renewable generation power plants with a total maximum capacity of 3500 MW and 3174 MW, respectively. Regular winds from the ocean provide a relatively steady production of wind power [26].

The results shown in this study correspond to a three-phase short-circuit in a transmission line connecting buses 5 and 6, adjacent to Bus 5, and cleared after 300 ms. This incident is chosen because it poses a considerable risk to transient stability due, on the one hand, to its location in the bulk of the transmission system, and on the other hand, to its proximity to the main synchronous power plants. Rotor angle deviation limits are reached at one or more synchronous generators in all the studied cases, affecting the optimal dispatch. This means that the solution given by a classical OPF is not transiently stable under the studied contingency and the TSCOPF modifies the power dispatch to provide a stable solution. Consequently, the total generation cost provided by a TSCOPF is higher than the cost of the dispatch provided by a classical OPF for selected contingencies.

The optimization problem is modeled in GAMS language [27] and solved using prime-dual interior point library IPOPT [28]. All simulations are performed using a personal computer based on Intel Core (TM) i7-2600 CPU 3.4 GHz, 16 GB RAM.

IV. Results and Discussion

A. Effect of non-synchronous generation on the transient stability.

This section presents several case studies in which non-synchronous renewable generation covers most of the demand of the system. The objective is to evaluate the effect of the substitution of synchronous power plants with non-synchronous generation on the dispatch and the total cost of generation. Different scenarios towards an objective of a 100% renewable system are evaluated:

- Case study 1: Current situation in which all synchronous power plants are available.
- Case study 2: Coal-fired power stations, which are the most polluting, are disconnected.
- Case study 3: Coal-fired power stations and combined-cycle power plants are disconnected, achieving a 100% renewable scenario in the region.

Table II shows the dispatch of synchronous power plants in the three cases together with their data. The available non-synchronous renewable resource is 2221.8 MW (over 70% of the installed nominal capacity) and supplies 86.7% of the demand. All available non-synchronous renewable generation is systematically dispatched. Results are obtained using: a) a classical OPF without dynamic constraints; b) a TSCOPF considering the three phase short-circuit in line 5-6 adjacent to bus 5 and no inertia emulation; and c) a TSCOPF considering the same contingency with non-synchronous power parks equipped with inertia emulation.

It can be seen in Table II that the classical OPF dispatches only plant G5 because it is the most economical. Application of the TSCOPF model, which takes into account the stability limits, indicates that the result given by the OPF is not stable under the considered contingency. The TSCOPF increases the total generation cost by 1220 M.U. with respect to the OPF because the algorithm assigns power generation to more expensive power plants to ensure stability. In the case TSCOPF-EMU, when non-synchronous power parks are equipped with inertia emulation, the system is more stable under the considered contingency and the cost increment is reduced from 1220 M.U. to 1133 M.U.

Regarding the results in the second case study, the OPF solution dispatches all the synchronous generation to the combined cycle plant connected to bus 11, which is the most economical. The application of the TSCOPF model increases the total generation cost by 2505 M.U. Similarly to the previous case, the introduction of the synthetic inertia reduces the total generation cost to 1488 M.U. over the cost given by the OPF.

The third case study presents a 100% renewable scenario, in which hydro generation provides the only synchronous generation in the area. Again, when using a classical OPF, all synchronous generation is dispatched to the most economic power plant, in this case to hydro plant G4. The application of a TSCOPF shifts 125.7 MW to the most expensive power plant to achieve a stable case under the considered contingency, increasing the total generation costs by 3348 M.U (increase of 14.2% over the OPF). Once again, when non-synchronous generation provides synthetic inertia the case is more stable, and the total generation cost to make the system stable is reduced to 2238 M.U. (increase of 9.5% over the OPF).

Fig. 2 and Fig. 3 show the differences in the response of hydro machines obtained as a result of a TSCOPF in the third case study. Fig. 2 shows the rotor angles of hydro power plants

This article has been accepted for publication in a future issue of this journal, but has not been fully edited. Content may change prior to final publication. Citation information: DOI 10.1109/TPWRS.2020.3022082, IEEE Transactions on Power Systems

TABLE II
RESULTS OF THE DISPATCH FOR SYNCHRONOUS POWER PLANTS UNDER THE THREE CASE STUDIES.

Power plant data								
Technology	Coal	Coal	Gas	Gas	Hydro	Hydro	**Cost (M.U.)**	**ΔCost (M.U.)**
Marginal cost (M.U./MWh)	29	38	51	63	72	98		
Nominal power (MW)	450	1400	350	700	400	200		
Minimum power (MW)	112.5	350	35	70	0	0		
Power plant	**G5 (MW)**	**G9 (MW)**	**G11 (MW)**	**G10 (MW)**	**G4 (MW)**	**G12 (MW)**		
Case study 1. All synchronous generation available								
OPF	327.4	ND[1]	ND[1]	ND[1]	ND[1]	ND[1]	9495	-
TSCOPF	274.3	ND[1]	54.2	ND[1]	ND[1]	ND[1]	10715	1220
TSCOPF EMU	277.8	ND[1]	50.4	ND[1]	ND[1]	ND[1]	10628	1133
Case study 2. Without coal								
OPF	NA[2]	NA[2]	327.4	ND[1]	ND[1]	ND[1]	16697	-
TSCOPF	NA[2]	NA[2]	211.1	ND[1]	117.2	ND[1]	19202	2505
TSCOPF EMU	NA[2]	NA[2]	208.7	119.7	ND[1]	ND[1]	18185	1488
Case study 3. 100 % renewable								
OPF	NA[2]	NA[2]	NA[2]	NA[2]	327.4	ND[1]	23572	-
TSCOPF	NA[2]	NA[2]	NA[2]	NA[2]	202.8	125.7	26920	3348
TSCOPF EMU	NA[2]	NA[2]	NA[2]	NA[2]	241.8	85.7	25810	2238

1. ND: Not dispatched
2. NA: Not applicable

when non-synchronous renewable power plants provide/do not provide synthetic inertia. Fig. 2 shows the rotor speed deviation of hydro power plants in the same scenarios. It can be seen, both in Fig. 2 and Fig. 3, that rotor angle and rotor speed oscillations are reduced when renewable power plants provide synthetic inertia. This results in a more stable situation and, consequently, a more economical operation as shown in Table II.

Fig. 4 analyzes deeply the third case of study, 100% renewable scenario in which power plants are equipped with inertia emulation. Fig. 4 shows the active power injected by the non-synchronous renewable plant connected to bus 6 together with the frequency at this bus as calculated by the frequency divider. It can be seen that during the voltage dip due to the short-circuit the plant reduces its output power. Once the fault is cleared, the plant modifies its active output power following the ROCOF as imposed by equations (10)-(13) to damp the electromechanical oscillations of the system.

Table III shows the execution times for all the case studies presented in Table II. In OPF cases, all times are less than 0.2s, while the two proposed TSCOPF variants present convergence times between 3.67 to 7.21 s. It must be pointed out that no convergence problems have been observed in the case studies.

B. Impact of non-synchronous generation in a 100% renewable scenario

This section analyses a scenario in which 100% of the generation in the North-West Spanish power system comes from renewable sources. As all fossil fuel power stations are

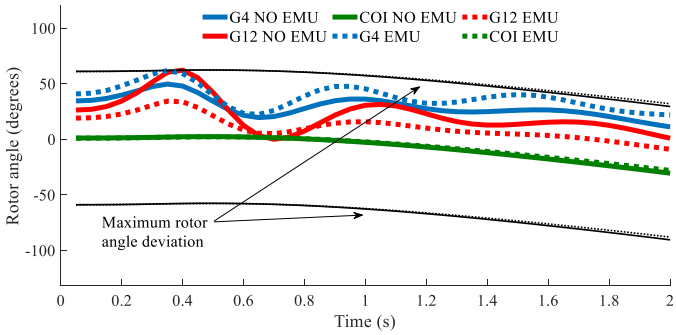

Fig. 2 Rotor angles of the synchronous power plants for a 100% renewable case without inertia emulation (NO EMU) and with inertia emulation (EMU).

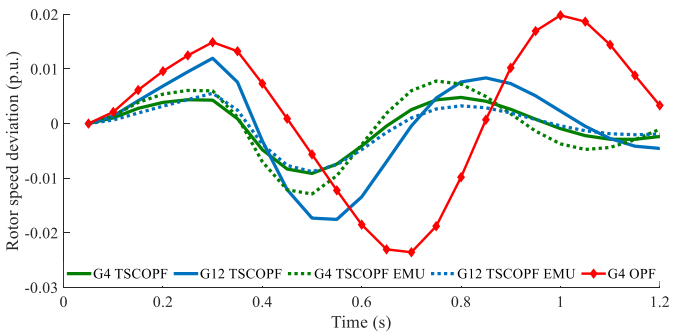

Fig. 3 Rotor speed deviation of the synchronous power plants for the 100% renewable: case study 3

This article has been accepted for publication in a future issue of this journal, but has not been fully edited. Content may change prior to final publication. Citation information: DOI 10.1109/TPWRS.2020.3022082, IEEE Transactions on Power Systems

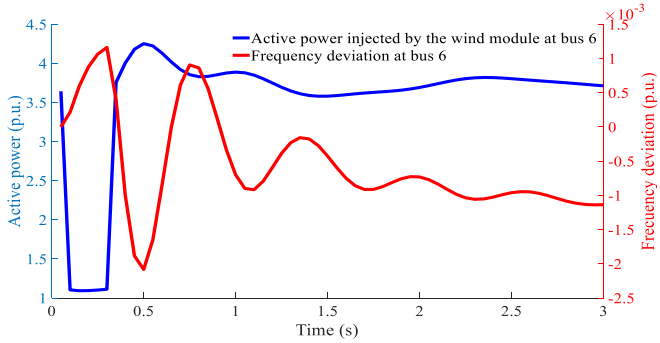

Fig. 4 Active generation and frequency at bus 6. Left axis: Active power of the non-synchronous renewable plant. Right axis: Frequency.

TABLE III
EXECUTION TIMES (S) FOR THE CASE STUDIES IN TABLE II

Algorithm	Case study 1	Case study 2	Case study 3
OPF	0.19	0.11	0.03
TSCOPF	7.1	3.67	7.2
TSCOPF EMU	4.35	7.21	4.14

disconnected from the studied area, the only remaining synchronous generators are the two hydro power plants connected at buses 4 and 12. Both hydro power plants can be dispatched depending on the availability of non-synchronous generation, with G4 taking precedence over G12 due to its lower generation cost. In section IV.A, the non-synchronous generation covers 86.7% of the demand. However, non-synchronous generation varies depending on the available wind and solar resource.

Table IV shows the results obtained when non-synchronous generation supplies 85%, 90% and 95% of the total generation in the area. As expected, the lowest generation costs correspond always to the optimal power flow algorithm because it does not consider stability constraints. When a short-circuit is applied to bus 5 and stability constraints are included in the model, the total generation cost increases because part of the generation needs to be shifted from G4 to G12 to keep the system stable. This effect is quite significant when no inertia emulation is applied (TSCOPF in Table IV), reaching 36.1% in the case of the maximum availability of non-synchronous power.

TABLE IV
OPTIMAL DISPATCH IN A 100% RENEWABLE SCENARIO

Algorithm	G4 (MW)	G12 (MW)	Cost (MU)	ΔCost (%)
85% non-synchronous - 15% hydroelectric				
OPF	357	0	25808	-
TSCOPF	227	132	29260	13.4
TSCOPF EMU	237	121	28947	12.2
90 % non-synchronous - 10% hydroelectric				
OPF	256	0	18466	-
TSCOPF	140	117	21577	16.8
TSCOPF EMU	241	15	18846	2.1
95 % non-synchronous - 5% hydroelectric				
OPF	129	0	9282	-
TSCOPF	4	126	12631	36.1
TSCOPF EMU	129	0	9282	0

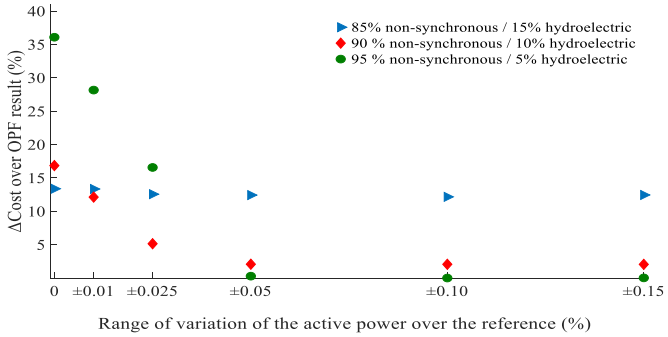

Fig. 5 Cost increment of the TSCOPF over the OPF for different scenarios of available renewable resources and parameters of synthetic inertia.

The application of an inertia emulation control that limits power deviation to 10% (TSCOPF EMU ±10% in Table IV) significantly reduces the cost by making it possible to increase the generation in hydro power plant G4. Therefore, non-synchronous power plants with inertia emulation help to maintain transient stability and low generation costs mainly with large shares of non-synchronous generation.

Constraints (11) and (12) limit the range of active power variation in the synthetic inertia control, which is a key aspect when designing the control strategy. Fig. 5 shows the increase in total generation cost in percentage, over a conventional OPF for a range of different values of saturation. It can be seen that the total generation cost decreases as the range increases from 0 to 5%. This is because the synthetic inertia effect makes the system more stable. However, limits on EMU above 5% cease to have a significant impact in the studied cases.

V. CONCLUSIONS

This paper proposes a TSCOPF model based on the simultaneous discretization method calculating frequency and voltages in all buses and sample times. The model includes a control for synthetic inertia in non-synchronous renewable generation. The following conclusions are drawn:

- The algorithm is successfully tested in the north-western Spanish system, providing a tool for calculating of the optimal operation of the system with high shares of non-synchronous renewable generation while maintaining economic and secure operation limits.
- Results show that inertia emulation in non-synchronous power plants affects transient stability and reduces the total generation cost that ensures stability. In the studied cases, the largest cost reductions are obtained when the share of non-synchronous generation increases.
- The effect of the parameters of the control of the synthetic inertia on transient stability can be evaluated using the proposed tool.
- No convergence issues have been observed in the case studies and the solution is reached in few seconds.

Future works are expected to be done, but not limited to, on the following research directions: 1) Evaluation of multi-step integration techniques to include the differential equations into

the optimization problem; 2) Implementation of an energy recovery function in the proposed model; 3) Optimization of parameters of synthetic inertia controls using a variant of the proposed tool; and 4) Collaboration with the system operator to test and further improve the proposed software tool.

VI. Acknowledgment

This work has been supported by the Spanish Ministry of Science and Innovation (ref. PID2019-104449RB-I00) within the 'Plan Estatal de Investigación Científica y Técnica y de Innovación 2017/2020'.

VII. References

[1] B. Kroposki *et al.*, "Achieving a 100% Renewable Grid: Operating Electric Power Systems with Extremely High Levels of Variable Renewable Energy," *IEEE Power and Energy Magazine*, vol. 15, no. 2, pp. 61–73, Mar. 2017, doi: 10.1109/MPE.2016.2637122.

[2] S. Abhyankar, G. Geng, M. Anitescu, X. Wang, and V. Dinavahi, "Solution techniques for transient stability-constrained optimal power flow – Part I," *IET Generation, Transmission & Distribution*, vol. 11, no. 12, pp. 3177–3185, Jun. 2017, doi: 10.1049/iet-gtd.2017.0345.

[3] G. Geng, S. Abhyankar, X. Wang, and V. Dinavahi, "Solution techniques for transient stability-constrained optimal power flow – Part II," *IET Generation, Transmission & Distribution*, vol. 11, no. 12, pp. 3186–3193, Jun. 2017, doi: 10.1049/iet-gtd.2017.0346.

[4] F. Capitanescu *et al.*, "State-of-the-art, challenges, and future trends in security constrained optimal power flow," *Electric Power Systems Research*, vol. 81, no. 8, pp. 1731–1741, Aug. 2011, doi: 10.1016/j.epsr.2011.04.003.

[5] Y. Xu, Z. Y. Dong, Z. Xu, R. Zhang, and K. P. Wong, "Power system transient stability-constrained optimal power flow: A comprehensive review," in *2012 IEEE Power and Energy Society General Meeting*, Jul. 2012, pp. 1–7, doi: 10.1109/PESGM.2012.6344753.

[6] J. Driesen and K. Visscher, "Virtual synchronous generators," in *2008 IEEE Power and Energy Society General Meeting - Conversion and Delivery of Electrical Energy in the 21st Century*, Jul. 2008, pp. 1–3, doi: 10.1109/PES.2008.4596800.

[7] ENTSO-E Guidance document for national, implementation for network codes on grid connection, and C. Broderick, "Need for synthetic inertia (SI) for frequency regulation," p. 9, Mar. 2017.

[8] M. Pertl, T. Weckesser, M. Rezkalla, and M. Marinelli, "Transient stability improvement: a review and comparison of conventional and renewable-based techniques for preventive and emergency control," *Electr Eng*, vol. 100, no. 3, pp. 1701–1718, Sep. 2018, doi: 10.1007/s00202-017-0648-6.

[9] ENTSO-E Guidance document for national and implementation for network codes on grid connection, "High Penetration of Power Electronic Interfaced Power Sources (HPoPEIPS)," *Power Sources*, p. 37, Mar. 2017.

[10] E. Rakhshani and P. Rodriguez, "Inertia Emulation in AC/DC Interconnected Power Systems Using Derivative Technique Considering Frequency Measurement Effects," *IEEE Transactions on Power Systems*, vol. 32, no. 5, pp. 3338–3351, Sep. 2017, doi: 10.1109/TPWRS.2016.2644698.

[11] F. M. Gonzalez-Longatt, "Impact of emulated inertia from wind power on under-frequency protection schemes of future power systems," *J. Mod. Power Syst. Clean Energy*, vol. 4, no. 2, pp. 211–218, Apr. 2016, doi: 10.1007/s40565-015-0143-x.

[12] R. Eriksson, N. Modig, and K. Elkington, "Synthetic inertia versus fast frequency response: a definition," *IET Renewable Power Generation*, vol. 12, no. 5, pp. 507–514, Sep. 2017, doi: 10.1049/iet-rpg.2017.0370.

[13] F. Milano and Á. Ortega, "Frequency Divider," *IEEE Transactions on Power Systems*, vol. 32, no. 2, pp. 1493–1501, Mar. 2017, doi: 10.1109/TPWRS.2016.2569563.

[14] C. Carrillo, J. Cidrás, E. Díaz-Dorado, and A. F. Obando-Montaño, "An Approach to Determine the Weibull Parameters for Wind Energy Analysis: The Case of Galicia (Spain)," *Energies*, vol. 7, no. 4, pp. 2676–2700, Apr. 2014, doi: 10.3390/en7042676.

[15] N. Hatziargyriou and A. Zervos, "Wind power development in Europe," *Proceedings of the IEEE*, vol. 89, no. 12, pp. 1765–1782, Dec. 2001, doi: 10.1109/5.975906.

[16] F. Arredondo, P. Ledesma, and E. D. Castronuovo, "Optimization of the operation of a flywheel to support stability and reduce generation costs using a Multi-Contingency TSCOPF with nonlinear loads," *International Journal of Electrical Power & Energy Systems*, vol. 104, pp. 69–77, Jan. 2019, doi: 10.1016/j.ijepes.2018.06.042.

[17] F. Arredondo, E. D. Castronuovo, P. Ledesma, and Z. Leonowicz, "Analysis of Numerical Methods to Include Dynamic Constraints in an Optimal Power Flow Model," *Energies*, vol. 12, no. 5, p. 885, Mar. 2019, doi: 10.3390/en12050885.

[18] Siemens Energy, Inc., *Siemens Power Technologies International, PSSE 34 Program Application Guide*. .

[19] P. Ledesma, F. Arredondo, and E. D. Castronuovo, "Optimal Curtailment of Non-Synchronous Renewable Generation on the Island of Tenerife Considering Steady State and Transient Stability Constraints," *Energies*, vol. 10, no. 11, p. 1926, Nov. 2017, doi: 10.3390/en10111926.

[20] Á. Ortega and F. Milano, "Comparison of different PLL implementations for frequency estimation and control," in *2018 18th International Conference on Harmonics and Quality of Power (ICHQP)*, May 2018, pp. 1–6, doi: 10.1109/ICHQP.2018.8378935.

[21] Á. Ortega, A. Musa, A. Monti, and F. Milano, "Hardware-in-the-Loop Validation of the Frequency Divider Formula," in *2018 IEEE Power Energy Society General Meeting (PESGM)*, Aug. 2018, pp. 1–5, doi: 10.1109/PESGM.2018.8586353.

[22] J. G. Slootweg, S. W. H. de Haan, H. Polinder, and W. L. Kling, "General model for representing variable speed wind turbines in power system dynamics simulations," *IEEE Transactions on Power Systems*, vol. 18, no. 1, pp. 144–151, Feb. 2003, doi: 10.1109/TPWRS.2002.807113.

[23] "Ministerio de Industria, Turismo y Comercio. P.O. 12.3 Requisitos de Respuesta Frente a Huecos de Tensión de las Instalaciones Eólicas." https://www.boe.es/boe/dias/2006/10/24/pdfs/A37017-37019.pdf.

[24] P. W. Sauer and M. A. Pai, "Power system dynamics and stability," *Urbana*, vol. 51, p. 61801, 1997.

[25] P. Kundur, N. J. Balu, and M. G. Lauby, *Power system stability and control*. McGraw-hill New York, 1994.

[26] "EGA, Asociación Eólica de Galicia." http://www.ega-asociacioneolicagalicia.es/es/elvientoengalicia/potencialeolico.php (accessed Oct. 23, 2017).

[27] "GAMS - Cutting Edge Modeling." https://www.gams.com/ (accessed Mar. 06, 2018).

[28] "Ipopt Documentation." https://coin-or.github.io/Ipopt/ (accessed Mar. 06, 2018).

VIII. Biographies

Francisco Arredondo Rodríguez received his Ph.D. in electrical engineering in 2019 at University Carlos III of Madrid, where he is currently an Assistant Professor. He has been an academic visitor at Wroclaw University of Technology, Poland. His research interest includes the power system stability, renewable generation, energy storage systems, and mathematical optimization methods.

Pablo Ledesma Larrea received his Ph.D. in 2001 at University Carlos III of Madrid, where he is currently an Associate Professor. He has worked with the Spanish TSO on several projects on large-scale integration of renewable energy. He has been an Academic Visitor at Chalmers University, Sweden and Strathclyde University, UK. His areas of research are transient stability and dynamic modeling of power systems.

Edgardo D. Castronuovo (M'03-SM'07) received a B.S. degree (1995) in Electrical Engineering from the National University of La Plata, Argentina; both M.Sc. (1997) and Ph.D. (2001) degrees from the Federal University of Santa Catarina, Brazil, and performed a Post-Doctorate (2005) at INESC-Porto, Portugal. He worked at the Power System areas of CEPEL, Brazil, and INESC-Porto, Portugal. Currently, Dr. Castronuovo is Head and Associate Professor at the Department of Electrical Engineering, University Carlos III of Madrid, Spain. His interests are in optimization methods applied to power system problems, renewable generation and storage

Mohammad Amin Aghahassani received his B.Sc. degree in Electrical Engineering from Amirkabir University of Technology, Tehran, Iran, in 2013, and the M.Sc. degree in Electrical Engineering from Polytechnic University of Milan, Italy, in 2017. He is currently pursuing a Ph.D. degree in electrical engineering at University Carlos III of Madrid, Spain. His research interests include power system optimization and stability analysis.